Formation of Peroxy Radicals from OH−Toluene Adducts and O_2

Birger Bohn

Institut für Chemie und Dynamik der Geosphäre, Institut II: Troposphäre, Forschungszentrum Jülich GmbH, D-52425 Jülich, Germany

Received: September 19, 2000; In Final Form: March 7, 2001

The gas-phase reaction of OH radicals with toluene and toluene-d_8 and reactions of the resulting OH adducts with O_2 were studied in N_2/O_2 mixtures at atmospheric pressure and room temperature. OH production was performed by pulsed 248 nm photolysis of H_2O_2. Cw UV-laser long-path absorption at 308 nm was used for time-resolved detection of OH and OH−toluene adducts. The reaction OH + toluene was studied in N_2 and O_2 and similar rate constants of $(5.70 \pm 0.19) \times 10^{-12}$ cm^3 s^{-1} (N_2) and $(5.60 \pm 0.14) \times 10^{-12}$ cm^3 s^{-1} (O_2) were obtained at 100 kPa. For toluene-d_8 the corresponding rate constants are $(5.34 \pm 0.34) \times 10^{-12}$ cm^3 s^{-1} (N_2) and $(5.47 \pm 0.14) \times 10^{-12}$ cm^3 s^{-1} (O_2). Absorption cross-sections of $(1.1 \pm 0.2) \times 10^{-17}$ cm^2 were determined for both the OH−toluene and OH−toluene-d_8 adduct at 308 nm. Rate constants of $(4.7 \pm 1.4) \times 10^{-11}$ cm^3 s^{-1} and $(1.8 \pm 0.5) \times 10^{-10}$ cm^3 s^{-1} were determined for the OH−toluene adduct self-reaction and the OH−toluene adduct + HO_2 reaction, respectively. Upper limits $\leq 8 \times 10^{-15}$ cm^3 s^{-1} were estimated for any reactions of the OH−toluene adduct with H_2O_2 or toluene. Adduct kinetics in the presence of O_2 is consistent with reversible formation of peroxy radicals with an estimated rate constant of $(3 \pm 2) \times 10^{-15}$ cm^3 s^{-1} and an equilibrium constant of $(3.25 \pm 0.33) \times 10^{-19}$ cm^3 (toluene-d_8: $(3.1 \pm 1.2) \times 10^{-19}$ cm^3). The effective adduct loss from the equilibrium can be explained by (i) an additional, irreversible reaction of the adduct with O_2 with a rate constant of $(6.0 \pm 0.5) \times 10^{-16}$ cm^3 s^{-1} (toluene-d_8: $(4.7 \pm 1.2) \times 10^{-16}$ cm^3 s^{-1}), or (ii) a unimolecular reaction of the peroxy radical, with a rate constant of $(1.85 \pm 0.15) \times 10^3$ s^{-1} (toluene-d_8: $(1.5 \pm 0.4) \times 10^3$ s^{-1}). Consequences for the atmospheric degradation of toluene will be discussed.

Introduction

Volatile aromatic compounds are emitted into the atmosphere by mainly anthropogenic sources such as combustion processes, vehicle emissions, and solvent use. Recent model calculations show that in urban areas up to 40% of photochemically produced ozone can be attributed to emissions of aromatics (benzene and alkylbenzenes) where toluene is the most important single compound.[1] However, a reliable assessment of photochemical ozone creation potentials depends on the knowledge of the correct and complete degradation mechanism, and considerable uncertainties still exist for aromatic compounds.

The first step of the tropospheric degradation of aromatics is reaction with OH radicals which is generally well understood.[2,3] OH reaction with toluene mainly proceeds by reversible addition leading to a methylhydroxycyclohexadienyl radical ($HO-C_6H_5-CH_3$, species (I) in Figure 1, referred to as adduct in the following):

$$OH + C_6H_5CH_3 \leftrightarrow HO-C_6H_5CH_3 \quad (R1a/-1a)$$

OH also reacts by H-atom abstraction which leads to benzyl radicals:

$$OH + C_6H_5CH_3 \rightarrow C_6H_5CH_2 + H_2O \quad (R1b)$$

Reaction 1b accounts for about 7% at room temperature finally yielding benzaldehyde under atmospheric conditions.[3]

In previous studies, reactions of the adduct with O_2, NO_2, and NO were studied by investigating the influence of the reactants on the equilibrium (R1a/−R1a) by monitoring OH.[4,5] The results showed that in the atmosphere decomposition of the adduct (−R1a) can be neglected and that the adduct reacts with O_2:

$$\text{adduct} + O_2 \rightarrow \text{products} \quad (R2)$$

Although reaction with NO_2 was found to be fast ($k = (3.6 \pm 0.4) \times 10^{-11}$ cm^3 s^{-1}),[4] Reaction 2, proceeding with a rate constant of $(5.4 \pm 0.6) \times 10^{-16}$ cm^3 s^{-1},[4] dominates due to the high atmospheric concentration of O_2. This conclusion was drawn from an extrapolation of experimental conditions (0.0−0.4 kPa of O_2)[4,5] to atmospheric conditions (20.5 kPa of O_2) and was confirmed by product studies at various NO_2 levels.[6] However, no further information on the reaction mechanism or the products of Reaction 2 could be derived from the kinetic experiments.[4,5]

Figure 1 summarizes the pathways currently under consideration for Reaction 2.[7] Product studies[3,8] showed that some 20% of the adducts (I) are converted to cresols (II) probably by abstraction of the redundant ring H-atom by O_2 forming HO_2. Based on theoretical considerations[9−11] it was thought that the remaining fraction of the adducts forms peroxy radicals (III) followed by reaction with NO or an intramolecular rearrangement reaction leading to a bicyclic radical (IV) which then forms a bicyclic peroxy radical (V) followed by reaction with NO. Both peroxy radical + NO reactions are thought to lead to high yields of HO_2 in consecutive reactions with O_2, partly after ring fragmentation.[7] However, the intermediates (III, IV, V) have

10.1021/jp0033972 CCC: $20.00
Published on Web 06/05/2001

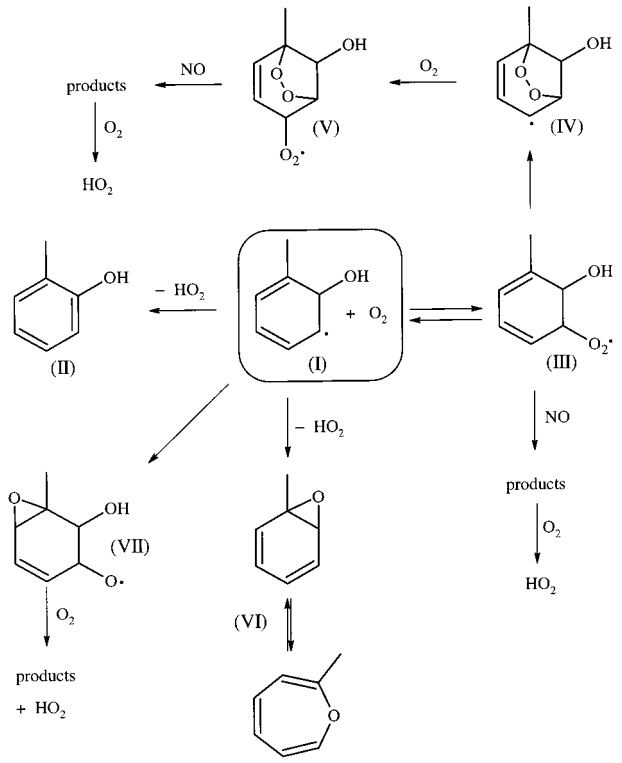

Figure 1. Reaction mechanism showing currently discussed reaction pathways of the OH−toluene adduct + O_2 reaction.[3,7,10−13] Formation of cresols (II), toluene oxide/methyloxepin (VI), and consecutive reactions of the epoxide−alkoxy radical (VII) are leading to HO_2 with no preceding NO reaction as opposed to HO_2 formation via the peroxy radicals (III) and (V).

not yet been detected directly in the gas phase and from the large variety of degradation products detected in smog chamber studies it is not possible to firmly conclude on the mechanism. The majority of secondarily formed stable compounds (e.g., ring-cleavage products such as unsaturated carbonyl compounds)[3] is very reactive toward OH and is also readily photolyzed. As a consequence, the carbon balance of typical product studies on aromatics is only about 50%[3] and the mechanism remained highly speculative.

More recently, formation of arene oxides (VI) + HO_2 in Reaction 2 has been proposed.[12,13] The degradation of these compounds by OH reaction, photolysis, and thermal decomposition was found to lead to products also observed in the OH initiated oxidation of aromatics.[12,13] Moreover, an apparently fast (not RO_2 + NO preceded) and virtually quantitative formation of HO_2 reported in other studies[14] can be explained by this mechanism. On the other hand, also a proposed formation of an epoxide−alkoxy radical (VII)[10] would (possibly after ring fragmentation) lead to a fast formation of HO_2 in consecutive reactions with O_2.[10,15] Thus, an investigation of the formation kinetics and yield of secondarily formed HO_2 in the presence of a large excess of O_2 could help to assess the relative importance of these recently proposed reaction pathways. However, as a prerequisite for such kind of studies the details of the kinetics of the adduct + O_2 reaction must be known.

By means of laser long-path absorption detection it was shown recently in this laboratory[16] that in the case of benzene the kinetics of the adduct at higher O_2 concentrations (up to 100 kPa) is consistent with a fast, reversible formation of a peroxy radical (corresponding to radical (III) in Figure 1, referred to as adduct-O_2 in the following):

$$\text{adduct} + O_2 \leftrightarrow \text{adduct}-O_2 \qquad \text{(R2a/−2a)}$$

The reversibility, also indicated in Figure 1, was predicted theoretically[9,17,18] and was known from liquid phase,[19] but the peroxy radical was found to be unexpectedly short-lived (2.5 ms in synthetic air) on account of competing loss processes of the adduct:

$$\text{adduct} + O_2 \rightarrow \text{other products} \qquad \text{(R2b)}$$

and/or the peroxy radical:

$$\text{adduct}-O_2 \rightarrow \text{other products} \qquad \text{(R3)}$$

In this work, these studies are extended and the kinetics of the OH−toluene and OH−toluene-d_8 adducts are investigated at high O_2 concentrations by long-path absorption.

Experimental Section

As in the previous study,[16] experiments were performed in a cylindrical 20 L glass cell in slowly flowing gas mixtures at atmospheric pressure (100 ± 2) kPa and room temperature (299 ± 2 K) (flow-rate about 3 L/min, STP). Calibrated mass-flow controllers (FC 260, Tylan) were used to prepare N_2/O_2 mixtures with varying amounts of O_2. The total pressure was measured with capacitance manometers (Baratron, MKS). The purity of the buffer gases was 99.999% (N_2) and 99.995% (O_2) (Messer Griesheim). Toluene and toluene-d_8 were introduced by purging the liquids in a thermostated gas saturator[20] at T = (279.9 ± 0.1) K. Toluene (Aldrich, 99+) and toluene-d_8 (Aldrich, 99+ at. % D) were used as purchased. The purity of the toluene sample was checked by GC analysis (99.98% + 0.02% of benzene).

Reactant concentrations were calculated from the ratio of the gas flows, the total pressure, and the vapor pressure of toluene at the temperature of the saturator (1.37 kPa).[21] Since no data for toluene-d_8 were available, the vapor pressures of toluene and toluene-d_8 were measured with capacitance manometers (Baratron, MKS) in a thermostated vacuum cell at about 279 K. The vapor pressure of toluene-d_8 was found to be higher by a factor of (1.04 ± 0.01) while the absolute value for toluene was within 5% of the literature data.[21] The ratio of 1.04 was then used to calculate toluene-d_8 concentrations at the actual temperature of the saturator. H_2O_2 was introduced by purging a preconcentrated solution at 298 K,[22] concentrations ranged between 3×10^{14} cm^{-3} and 1.1×10^{15} cm^{-3}. H_2O_2 concentrations were calculated from OH decay rates in the absence of other reactants using the current NASA-JPL recommendation for the rate constant of the OH + H_2O_2 reaction (1.7×10^{-12} cm^3 s^{-1}).[23]

OH was produced by pulsed laser-photolysis of H_2O_2 at 248 nm at a typical fluence of 1.5 mJ cm^{-2} and a repetition rate of 0.2 s^{-1}. With the H_2O_2 concentrations used this resulted in typical OH starting concentrations of about 1.5×10^{11} cm^{-3}. Pseudo-first-order conditions are assumed to apply for OH under all conditions. For the adduct the same assumption is made except in the absence of O_2 where OH starting concentrations were higher (see Results section on the absorption cross section of the adduct) and the lifetime of the adduct was long enough to allow radical−radical reactions to influence the time dependence (see Results section on the self-reaction of the adduct). Time-resolved monitoring of OH was made by cw UV-laser long-path absorption on the $Q_1(2)$ rotational line of the OH-($A^2\Sigma^+ \leftarrow X^2\Pi$)-transition at 307.995 nm (air) with a folded path-length of 100 m (100 reflections).[24] The typical laser power

TABLE 1: Rate Constants of OH + C_7H_8 and OH + C_7D_8 in Different Buffer Gases at (299 ± 2) K and Atmospheric Pressure

buffer gas	N^a	$[C_7H_8]/10^{14}$ cm^{-3}	$[H_2O_2]/10^{14}$ cm^{-3}	$k_1/^b10^{-12}$ cm^3 s^{-1}
		toluene		
O_2	7	0.0−8.3	5.7	5.60 ± 0.14
				5.73 ± 0.17[c]
N_2	7	0.0−8.3	5.9	5.82 ± 0.54[d]
				5.64 ± 0.13[e]
			average (N_2):	5.70 ± 0.19
		toluene-d_8		
O_2	7	0.0−6.9	4.7	5.47 ± 0.14
				5.33 ± 0.24[c]
N_2	4	0.0−6.9	4.9	5.43 ± 0.61[d]
				5.31 ± 0.35[e]
			average (N_2):	5.34 ± 0.34

[a] Number of data points/levels of toluene. [b] 2σ error limits (statistical). [c] $^1k_{OH}$ from monoexponential fits to difference signals (total − adduct). [d] $^1k_{OH}$ from biexponential fits to adduct signals. [e] $^1k_{OH}$ from biexponential fits to total signals.

was 200 μW at a line-width of about 500 kHz. OH−toluene adducts were detected −0.045 nm off the OH-line. In contrast to OH, the spectrum of the adduct is a broad continuum[25] upon which the sharp OH lines appear (dependent on reaction time, more details are given in the Results section). OH decay curves were recorded by averaging over 3−10 single measurements. Adduct decay curves were averaged over 10−200 single measurements, dependent on O_2 concentration. After 10−20 laser pulses, 5−10 min were allowed to elapse to prevent accumulation and photolysis of reaction and/or photolysis products.

Results

Rate Constants of OH + Toluene. The reaction of OH with toluene and toluene-d_8 was studied in N_2 and O_2. These measurements were made to rule out any difference of the OH kinetics in N_2 and O_2.

In O_2 OH signals I_{OH} decay monoexponentially since the underlying adduct absorption is negligible (see subsection on adduct kinetics in the presence of O_2) and decomposition of the adduct back to OH and toluene (Reaction −1a) is slow (about 3 s^{-1} at 298 K)[4] and can be neglected on account of the high toluene concentrations:

$$I_{OH} = I_{OH,0} \exp(-^1k_{OH}t) + C_{OH} \quad (1)$$

In this equation $^1k_{OH}$ is the first-order decay rate of OH and C_{OH} is the experimental background (usually less than ±1% of $I_{OH,0}$). Three-parameter fits of eq 1 were made for each decay curve, and rate constants of Reaction 1 were determined from a linear regression of OH decay rates as a function of toluene concentration. Rate constants k_1(toluene) = (5.60 ± 0.14) × 10^{-12} cm^3 s^{-1} and k_1(toluene-d_8) = (5.47 ± 0.14) × 10^{-12} cm^3 s^{-1} (2σ error limits) were obtained. Concentration ranges and experimental conditions are given in Table 1.

In N_2 the situation is more complicated due to the underlying absorption of the adduct. Absorption signals with the laser tuned on the OH line clearly do not decay monoexponentially as illustrated in Figure 2 (curves (a) and (b)). Also shown in Figure 2 are absorption traces with the laser tuned off the OH line by −0.045 nm which represent the adduct absorption alone (curves (c) and (d)). On the time-scale of the OH decays a decrease of these signals is hardly recognizable.

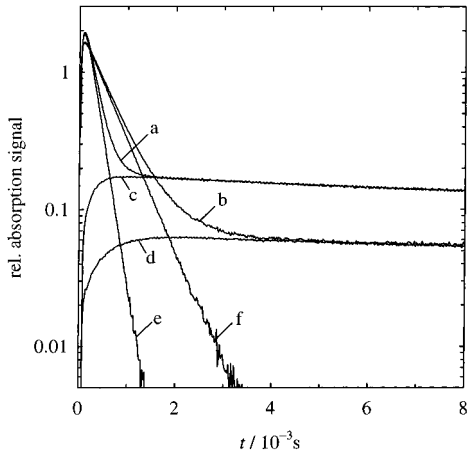

Figure 2. Time-dependent absorption signals in N_2 with the detection laser tuned on the OH absorption line (a, b) (signal from OH + adduct) and off the OH absorption line (c, d) (signal from adduct) averaged from 20 and 40 single experiments, respectively. The differences (e = a − c, f = b − d) correspond to the OH signal. Experimental conditions: $[H_2O_2] = 5.9 \times 10^{14}$ cm^{-3}, $[C_7H_8] = 6.9 \times 10^{14}$ cm^{-3} (a, c, e), and 1.6×10^{14} cm^{-3} (b, d, f).

Different methods were applied to determine the OH decay rates in N_2. First, the adduct absorption was subtracted from the total signal and OH decay rates were determined by fitting eq 1 to the differences. This method is justified because the differences exhibit no deviation from monoexponential decays as shown in Figure 2 (curves (e) and (f)), i.e., the adduct absorption is constant in this narrow wavelength range. The resulting rate constants k_1 are listed in Table 1.

Second, rise-and-fall type biexponential expressions were fitted to the adduct absorption signals:

$$I_{add} = I_{add,1} \exp(-^1k_{add}t) - I_{add,2} \exp(-^1k_{add,r}t) + C_{add} \quad (2)$$

The adduct rising rates $^1k_{add,r}$ are expected to correspond to the OH decay rates and similar rate constants k_1 were indeed obtained (Table 1). However, the accuracy of the rising rates is poorer due to the lower absorption signal of the adduct compared with OH. It should also be noted that, except from the rising part, eq 2 is an empirical description of the adduct decays for the present purpose only, i.e., neither is $^1k_{add}$ the actual decay rate of the adduct nor is C_{add} the actual background (see subsection on the self-reaction of the adduct).

Finally, biexponential expressions (sum of two exponentials as in eq 2 + constant) were fitted to the total signal. If eqs 1 and 2 are added and $^1k_{add,r} = {}^1k_{OH}$ is inserted, a biexponential expression results with the larger decay rate corresponding to the OH decay rate. The resulting rate constants k_1 are again very similar and given in Table 1. The latter method was also used in ref 16 to determine the rate constant of the OH + benzene reaction in N_2.

Considering the different statistical errors, weighted averages k_1(toluene) = (5.70 ± 0.19) × 10^{-12} cm^3 s^{-1} and k_1(toluene-d_8) = (5.34 ± 0.34) × 10^{-12} cm^3 s^{-1} were calculated for the rate constants in N_2.

Absorption Cross Section of the Adduct. The measurements described so far were also used to determine the absorption cross sections of the adducts at 308 nm from a comparison of OH and adduct absorption signals in N_2. The ratio of absorption cross sections was calculated using the following equation:

$$\frac{\sigma_{OH}}{\sigma_{add}} = \frac{f_1 f_2 I_{OH,0}}{f_3 I_{add,1} + C_{add}} \quad (3)$$

The factors f_1 and f_2 are correcting the OH signal I_{OH} (eq 1) with respect to the rise-time of the detection system and the fraction of OH which reacts with toluene (i.e., not with H_2O_2). The rise-time ($\tau_{rise} \approx 25$ μs, see Figure 2) does not affect the fitted OH decay rates if the first few data points at $t \leq 0.2$ ms are omitted in the fits of eq 1. However, $I_{OH,0}$ increases with increasing rise-time which is corrected by f_1:[26]

$$f_1 = 1 - {}^1k_{OH}\tau_{rise} \quad (4)$$

f_2 is calculated using the data of Table 1:

$$f_2 = \frac{k_1[C_7H_8]}{{}^1k_{OH}} \quad (5)$$

f_3 corrects the adduct signal with respect to the adduct rising rate in a similar fashion as f_1 considers τ_{rise}:

$$f_3 = 1 - {}^1k_{add}/{}^1k_{add,r} \quad (6)$$

The f_3 are very close to unity here (≥ 0.96) since ${}^1k_{add}$ is low. However, in the presence of O_2, where ${}^1k_{add}$ is increased it will be more significant (see subsection on the adduct kinetics in the presence of O_2).

Table 2 gives a summary of the data. The ratios of absorption cross sections were found to be similar for toluene and toluene-d_8 adducts and independent of the reactant concentrations. The averages were used to calculate absolute absorption cross sections using $\sigma_{OH} = 1.57 \times 10^{-16}$ cm^2 at the center of the OH $Q_1(2)$ line (100 kPa of N_2)[27] which leads to $\sigma_{add} = (1.08 \pm 0.06) \times 10^{-17}$ cm^2 for both adducts. However, in this procedure adduct yields of unity are assumed for Reaction 1. Benzyl radicals are also formed with a yield of about 7%, at least in the case of toluene.[3] From a published spectrum[25] an absorption cross section of about 7×10^{-18} cm^2 is estimated for the benzyl radical at 308 nm which leads to a minor correction of +3%. In the case of toluene-d_8 no such correction is possible since the absorption cross section of deuterated benzyl radicals is unknown. On the other hand, the yield of benzyl radicals is probably lower[2,28] ($\approx$2%, see Discussion section on the OH + toluene-d_8 reaction). Considering experimental errors $\sigma_{add} = (1.1 \pm 0.2) \times 10^{-17}$ cm^2 is finally determined for the absorption cross-sections of both adducts.

As is evident from Table 2, the initial OH concentration increases strongly with toluene concentration. A possible explanation for this effect (also observed with benzene)[16] is a sensitized dissociation of H_2O_2 by electronically excited triplet states of toluene following 248 nm excitation by the photolysis laser. In the presence of the lowest O_2 concentration (0.4 kPa) the effect vanishes while the OH kinetics and the ratio of the absorption signals are not affected by the increase of initial OH. Thus, it is considered a fast additional OH source not interfering with the reactions investigated in this work.

Adduct Kinetics in the Absence of O_2—Self-Reaction and Reaction with HO_2. Figure 3 shows decay curves of the adduct absorption in N_2 at a much longer time-scale than Figure 2. The absorption signals were converted to absolute concentrations with the absorption cross-section obtained above. The decays are clearly not exponential indicating the influence of an adduct self-reaction.

$$\text{adduct} + \text{adduct} \rightarrow \text{products} \quad (R4)$$

TABLE 2: First-Order OH Decay Rates ${}^1k_{OH}$, Initial OH Absorption Signals $I_{OH,0}$, Correction Factors for OH Signals f_1, f_2 (see text) and Ratios of OH and Adduct Absorption Cross Sections σ_{OH}/σ_{Add} at Different Toluene Concentrations

	${}^1k_{OH}$/[a] 10^3 s^{-1}	$I_{OH,0}$/ arb. units	f_1	f_2	σ_{OH}/σ_{add}
$[C_7H_8]/10^{14}$ cm^{-3}					
0.0	1.00	1.48	0.98	0.00	
1.61	1.90	2.14	0.95	0.48	14.6
3.02	2.71	2.57	0.93	0.63	13.8
4.27	3.54	2.93	0.91	0.72	14.7
5.71	4.24	3.67	0.89	0.77	14.8
6.89	4.93	3.98	0.88	0.80	15.5
8.29	5.75	3.99	0.86	0.83	14.2
				average:	14.6 ± 0.8[b]
$[C_7D_8]/10^{14}$ cm^{-3}					
0.0	0.83	0.94	0.98	0.00	-
2.50	2.23	1.48	0.94	0.63	13.8
4.72	3.40	2.11	0.92	0.76	15.0
6.92	4.50	2.69	0.89	0.82	15.3
				average:	14.6 ± 0.8[b]

[a] From difference signals (total-adduct), see Table 1. [b] Error limit covers largest deviation.

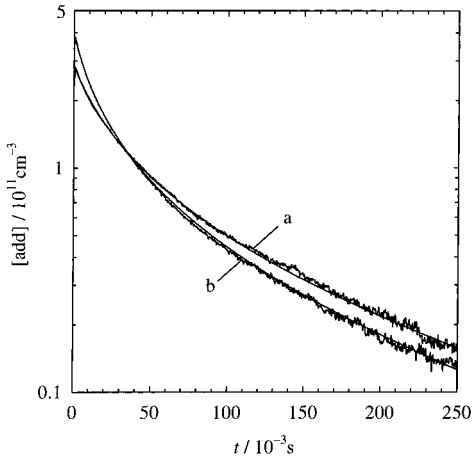

Figure 3. Adduct decay curves in N_2 averaged from 70 single experiments. Absolute concentrations were calculated using $\sigma_{add} = 1.1 \times 10^{-17}$ cm^2. The smooth curves show the result of a numerical fit considering a total of nine decay curves (see text). The crossing of the curves is attributable to a fast adduct + HO_2 Reaction 7. Experimental conditions: $[C_7H_8] = 1.09 \times 10^{14}$ cm^{-3}, $[H_2O_2] = 5.9 \times 10^{14}$ cm^{-3} (a), $[H_2O_2] = 1.15 \times 10^{15}$ cm^{-3} (b).

An attempt to extract the rate constant of Reaction 4 was to use a model which, in addition to Reaction 4, considers a first-order loss of the adduct for example by diffusion or reaction with impurities, with rate constant ${}^1k^0_{add}$. This leads to the following analytical solution of the time dependence (omitting the rising part of the decay curves at $t \leq 2$ ms):[16]

$$[\text{add}] = \frac{[\text{add}]_0 \, {}^1k^0_{add} \exp(-{}^1k^0_{add} t)}{{}^1k^0_{add} + 2[\text{add}]_0 k_4 (1 - \exp(-{}^1k^0_{add} t))} \quad (7)$$

where $[\text{add}]_0$ is the extrapolated adduct concentration at $t = 0$. Fits of eq 7 were made for nine decay curves obtained with two toluene concentrations (5.7×10^{14} cm^{-3} and 1.08×10^{15} cm^{-3}) and three H_2O_2 concentrations (3.3×10^{14} cm^{-3}, 5.9×10^{14} cm^{-3} and 1.14×10^{15} cm^{-3}) covering a range of adduct starting concentrations of $(1.3-4.2) \times 10^{11}$ cm^{-3}. The averages of the fitted rate constants k_4 and ${}^1k^0_{add}$ are listed in Table 3. ${}^1k^0_{add}$ was not increased if both $[H_2O_2]$ and $[C_7H_8]$ were doubled from which upper limits of 8×10^{-15} cm^3 s^{-1} were estimated for the rate constants of the reactions:

TABLE 3: Fitted Rate Constants of the Adduct + Adduct Self Reaction 4, the Adduct + HO_2 Reaction 7, and First-Order Loss Rate Constant $^1k^0_{add}$ from Different Methods of Data Analysis. The Data Obtained with Benzene in Ref 16 Were Reanalyzed for Direct Comparison

fitting method	k_4/ 10^{-11} cm^3 s^{-1}	k_7/ 10^{-11} cm^3 s^{-1}	$^1k^0_{add}$/ s^{-1}
	toluene		
single, average[a]	6.2 ± 1.8		4 ± 4
single, extrapolated[b]	4.1 ± 0.5		
total[c]	7.0	0.0(fixed)	1.3
total[c,d]	4.7	18	4.3
	4.7 ± 1.4[e]	18 ± 5[e]	
	benzene		
single, average[a]	3.8 ± 1.1[f]		8 ± 8[f]
single, extrapolated[b]	3.4 ± 1.0[f]		
total[c]	3.6	0.0(fixed)	10
total[c,g]	2.8	6.9	5.8
	2.8 ± 1.2[e]	7 ± 4[e]	

[a] Using eq 7, error limits cover largest deviation. [b] From linear extrapolation to $[HO_2]_0/[add]_0 = 0$, 2σ-error limits. [c] Numerical fits to all decay curves simultaneously, see text. [d] χ^2 decreases by a factor of 2.0 relative to run with fixed $k_7 = 0$. [e] Error bars estimated including uncertainty of σ_{add}. [f] Result of ref 16. [g] χ^2 decreases by a factor of 1.3 relative to run with fixed k_7=0.

$$\text{adduct} + C_7H_8 \rightarrow \text{products} \qquad \text{(R5)}$$

$$\text{adduct} + H_2O_2 \rightarrow \text{products} \qquad \text{(R6)}$$

On the other hand, the rate constants k_4 showed a marked increase with the ratio $[HO_2]_0/[add]_0$ (HO_2 from OH + H_2O_2) which indicates the influence of a fast reaction:

$$\text{adduct} + HO_2 \rightarrow \text{products} \qquad \text{(R7)}$$

The influence of Reaction 7 can also be recognized in Figure 3 where it leads to a crossing of the decay curves.

It is not possible to extract both k_4 and k_7 from single adduct decay curves. In ref 16, where the corresponding data on benzene were analyzed, the k_4 obtained using eq 7 were plotted against $[HO_2]_0/[add]_0$ and a linear extrapolation to $[HO_2]_0/[add]_0 = 0$ was made to eliminate the influence of HO_2. For comparison this procedure was also adopted here (see Table 3) where a range of starting concentration ratios $[HO_2]_0/[add]_0$ of 0.09−0.32 is covered by the nine decay curves under consideration. However, on account of the stronger effect a different method of data analysis was feasible: the decay curves were analyzed simultaneously by applying a numerical method (FACSIMILE)[29] in which the rate constants k_4, k_7, and $^1k^0_{add}$ were optimized as well the initial adduct concentration and the background of each curve. For comparison with the simpler approach (averaged k_4) the fit was also made with k_7 set to zero which gave a rather similar rate constant k_4 as compared to the average obtained above. Optimizing also k_7 improved the quality of the fit noticeable by a decrease of the residual sum of squares χ^2 by a factor of 2 (Table 3). Rate constants $k_4 = (4.7 \pm 1.4) \times 10^{-11}$ cm^3 s^{-1} and $k_7 = (1.8 \pm 0.5) \times 10^{-10}$ cm^3 s^{-1} were obtained in this run. The error limits were estimated by taking into account the strong mutual dependence of the rate constants as well as the uncertainty of the absorption cross section.

The same procedure was repeated with the benzene adduct data of ref 16 which leads to a minor revision of the self-reaction rate constant: k_4 (benzene) $= (2.8 \pm 1.2) \times 10^{-11}$ cm^3 s^{-1}. In comparison with toluene the influence of HO_2 is much smaller. As a consequence, only a rough estimate k_7 (benzene) $= (7 \pm 4) \times 10^{-11}$ cm^3 s^{-1} can be derived for the rate constant of the adduct + HO_2 reaction. The self-reaction of the toluene-d_8 adduct was not studied.

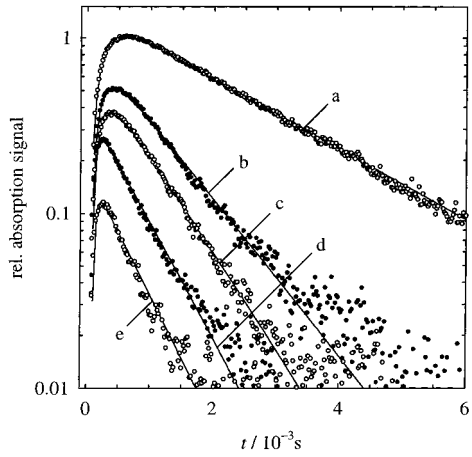

Figure 4. Adduct/peroxy radical decay curves and fitted biexponential decays (full lines) at various O_2 concentrations. Backgrounds were subtracted and the curves were normalized to the same amount of converted OH, i.e., the absorption signal decreases with increasing O_2 concentration. $[O_2]/10^{18}$ cm^{-3}: 1.03 (a), 3.83 (b), 6.46 (c), 11.7 (d), and 24.3 (e). Experimental conditions are listed in Table 4.

Adduct Kinetics in the Presence of O_2—Peroxy Radical Formation. Upon addition of O_2, adduct concentrations decay more rapidly indicating a reaction of the adduct with O_2. Figure 4 shows examples of decay curves at different O_2 concentrations. Note the shorter time-scale as compared to Figure 3. As mentioned above, the increase of OH starting concentrations with toluene concentration vanishes in the presence of O_2. As a consequence the influence of the adduct self-reaction can be neglected at $[O_2] \geq 2.0 \times 10^{17}$ cm^{-3}, and biexponential fits according to eq 2 were made to determine rising and decay rates. The fits are also shown in Figure 4. Measurements were made at O_2 concentrations of up to 2.4×10^{19} cm^{-3} (18 measurements with toluene, 6 with toluene-d_8, see Table 4), and for each decay curve also an OH decay curve was recorded.

As in the case of benzene[16] the obtained data are inconsistent with an irreversible adduct + O_2 reaction. First, the decay rates increase nonlinearly with O_2 concentration which is shown in Figure 5. Only at $[O_2] \leq 2.0 \times 10^{18}$ cm^{-3} the increase is approximately linear in accordance with the results of other studies made at low O_2 concentrations[4,5] (dashed line in Figure 5). Second, the apparent absorption cross sections (obtained using eq 3) decrease nonlinearly with O_2 as shown in Figure 6 and also recognizable in Figure 4. Both effects can be explained by the reaction model already outlined in the Introduction section, i.e., a reversible formation of a peroxy radical. With increasing O_2 concentration the equilibrium is shifted toward the peroxy radical which leads to a decrease of absorption signals since this species absorbs less strongly at 308 nm. Correspondingly, the measured decay rates are effective first-order loss rate constants of both species in equilibrium caused by either competing adduct + O_2 reactions (summarized as Reaction 2b) or decomposition reactions of the peroxy radical not leading back to the adduct (Reaction 3).

Effective Decay Rates

Assuming a fast equilibrium, i.e., if Reactions 2a/−2a are much faster than Reactions 2b or 3, a simplified expression can be derived for the effective adduct/peroxy radical decay rates as a function of O_2 concentration:[16]

TABLE 4: First-Order Effective Loss Rate Constants $^1k^{eff}$ and Effective Ratio σ_{OH}/σ^{eff} of OH and Adduct/Peroxy Radical Absorption Cross Sections at Different O_2 Concentrations

$[O_2]/10^{18}$ cm^{-3}	$[C_7H_8]/10^{14}$ cm^{-3}	$[H_2O_2]/10^{14}$ cm^{-3}	$^1k^{eff}/10^3$ s^{-1}	σ_{OH}/σ^{eff}
0.00			0.004[a]	14.6[b]
0.0995	5.7	5.7	0.053	15.3
0.211	5.6	5.7	0.129	16.9
0.327	5.6	5.7	0.170	17.4
0.439	5.6	5.7	0.234	18.5
0.597	5.7	6.3	0.323	16.7
0.991	5.6	11.3	0.414	16.3
1.03	5.7	6.3	0.462	18.6
1.48	5.6	6.3	0.607	21.5
1.88	5.7	6.3	0.791	22.2
2.29	5.7	11.3	0.800	20.0
3.53	5.6	11.3	0.933	25.3
3.83	5.7	6.3	1.02	28.2
4.88[c]	5.2	4.3	1.08	
6.46	5.7	6.3	1.26	35.6
11.7	10.8	10.4	1.51	52.6
11.9	5.7	6.3	1.41	58.5
24.2	10.7	10.4	1.67	90.9
24.3	10.7	10.4	1.66	90.9
$[O_2]/10^{18}$ cm^{-3}	$[C_7D_8]/10^{14}$ cm^{-3}	$[H_2O_2]/10^{14}$ cm^{-3}	$^1k^{eff}/10^3$ s^{-1}	σ_{OH}/σ^{eff}
0.00				14.6[b]
0.401	5.9	6.1	0.194	14.6
0.779	5.9	6.1	0.279	17.3
1.26	5.9	6.1	0.461	20.8
1.76	5.5	5.7	0.547	22.6
4.89	5.7	5.9	0.849	34.5
11.5	5.5	5.7	1.21	62.9

[a] See Table 3. [b] See Table 1. [c] 20 kPa total pressure.

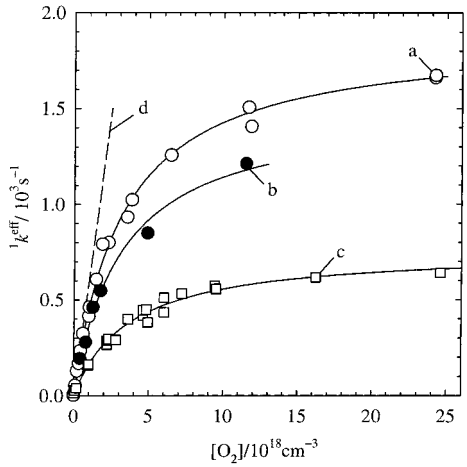

Figure 5. O_2 concentration dependence of effective decay rates from biexponential fits. Full lines are fits to eq 8. (a) Toluene, (b) toluene-d_8, (c) benzene (ref 16). The dashed line (d) indicates the limiting slope at low O_2 (toluene) corresponding to a rate constant of 6.0×10^{-16} cm^3 s^{-1}.

$$^1k^{\text{eff}} = \frac{[O_2](K_{2a}\,^1k_3 + k_{2b})}{1 + K_{2a}[O_2]} \tag{8}$$

where K_{2a} is the equilibrium constant:

$$K_{2a} = \frac{k_{2a}}{^1k_{-2a}} \tag{9}$$

Fits of eq 8 to the rate constants listed in Table 4 gave

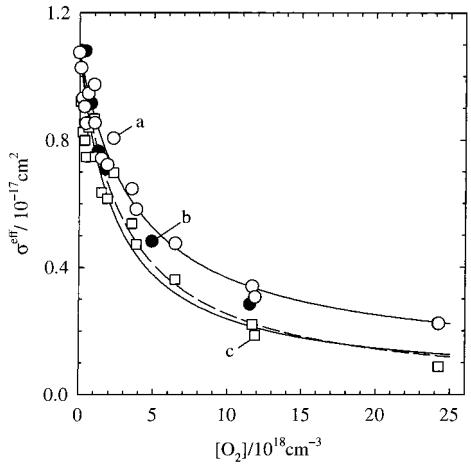

Figure 6. O_2 concentration dependence of effective absorption cross sections obtained using eq 3 and literature values of σ_{OH} (including the weaker pressure broadening in O_2).[27] (a) Toluene, (b) toluene-d_8, (c) toluene, not considering the unknown background signal (see text). The full lines are fits to eq 10, the dashed line shows the expected behavior with negligible absorption by the peroxy radical, and $K_{2a} = 3.25 \times 10^{-19}$ cm^3 (see text).

equilibrium constants K_{2a}(toluene) $= (3.25 \pm 0.33) \times 10^{-19}$ cm^3 and K_{2a}(toluene-d_8) $= (3.1 \pm 1.2) \times 10^{-19}$ cm^3. For the loss terms ($K_{2a}\,^1k_3 + k_{2b}$) in the numerator of eq 8, $(6.0 \pm 0.5) \times 10^{-16}$ cm^3 s^{-1} (toluene) and $(4.7 \pm 1.2) \times 10^{-16}$ cm^3 s^{-1} (toluene-d_8) were obtained (2σ error limits). The full lines in Figure 5 show the corresponding fits.

It should be noted that Reactions 2b and 3 cannot be distinguished because the sum term ($K_{2a}\,^1k_3 + k_{2b}$) cannot be separated, i.e., it cannot be decided on which side the loss occurs if the equilibrium between the radical species is fast. Assuming $^1k_3 = 0$ leads to an upper limit $k_{2b} = (6.0 \pm 0.5) \times 10^{-16}$ cm^3 s^{-1} while assuming $k_{2b} = 0$ leads to an upper limit $^1k_3 = (1.85 \pm 0.15) \times 10^3$ s^{-1}. Any intermediate case is possible.

An upper limit of 1×10^{-17} cm^3 s^{-1} is estimated for the rate constant of any reaction of the peroxy radical with O_2,

$$\text{adduct-O}_2 + \text{O}_2 \rightarrow \text{products} \tag{R8}$$

which would lead to a linear increase of the effective rate constants also toward high O_2 concentrations.[16] A spot check measurement at a total pressure of 20.5 kPa in pure O_2 gave a similar decay rate as in synthetic air at atmospheric pressure, i.e., in this range the total pressure does not affect the kinetics. Nevertheless, the decay rates listed in Table 4 could be biased by three effects.

First, there is an unknown background signal. An example of the magnitude of this signal (subtracted in Figure 4) is shown in Figure 7. The background did not increase with O_2 concentration but its relative importance increases with O_2 concentration since the adduct/peroxy radical absorption decreases. In the case of benzene a similar signal was observed but it was lower.[16] The nature of the background is unknown and there is no way to separate it from the adduct/peroxy radical absorption at short times. Also in the absence of H_2O_2 a small signal was observed which appeared within 0.5 ms after the laser pulse. However, its contribution to the background observed in the presence of H_2O_2 is not more than 20%. Thus, the background results mainly from products of an OH reaction or from more stable secondary products of adduct or peroxy radical reactions. In the first case (OH reaction) it would rise quickly and would not influence the decay of the adduct, in the latter case its rising rate would be similar to the adduct decay rate and a biexpo-

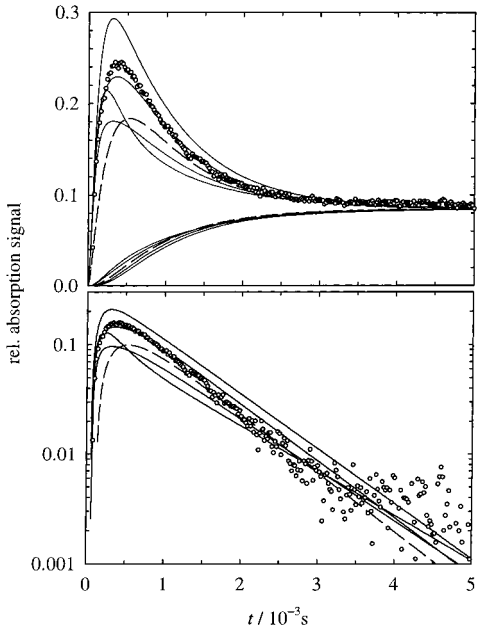

Figure 7. Experimental and simulated absorption traces at an O_2 concentration of 6.46×10^{18} cm^{-3}. Full lines show simulated curves for different values of k_{2a} and ${}^1k_{-2a}$ ($= k_{2a}/K_{2a}$) and the limiting cases ${}^1k_3 = 0$ or $k_{2b} = 0$. From top to bottom: ($k_{2a} = 1 \times 10^{-15}$ cm^3 s^{-1}, $k_{2b} = 0$), ($k_{2a} = 2 \times 10^{-15}$ cm^3 s^{-1}, $k_{2b} = 0$), ($k_{2a} = 1 \times 10^{-15}$ cm^3 s^{-1}, ${}^1k_3 = 0$), ($k_{2a} = 2 \times 10^{-15}$ cm^3 s^{-1}, ${}^1k_3 = 0$). Dashed line: limiting behavior for both cases at large k_{2a} and ${}^1k_{-2a}$ (fast equilibrium). Upper panel: Linear plot showing simulated total absorption signals as well as the magnitude of the experimental background absorption and its simulated built-up as a product of Reactions 2b or 3. Lower panel: Semilogarithmic plot with the final background subtracted. The differences in the final slopes indicate the influence of k_{2a} and ${}^1k_{-2a}$ on effective decay rates obtained from biexponential fits.

nential fit would still give the correct decay rate (as in the case of the biexponential fit to the total signal (OH + adduct) in N_2, see subsection on OH + toluene reaction). This possible time behavior is shown in Figure 7 (see below). However, a delayed formation of the background cannot be excluded. Such a delay would have two effects: the fitted decay rates would be larger and the decay curves would exhibit a minimum. Since no minimum was observed within experimental scatter, the possible increase of the decay rates due to a delayed formation of the background is estimated to be below 30% at the highest O_2 concentration where the relative influence of the background is strongest.

Second, there are indications that the rate constants k_{2a} and ${}^1k_{-2a}$ are not large enough to produce the idealized fast equilibrium needed to derive eq 8. In the absence of O_2 the adduct rising rates were similar to the OH decay rates (see subsection on OH + toluene reaction). This is also expected in the presence of O_2 if the equilibrium (2a/−2a) is fast. However, a deviation from this behavior was observed which became more pronounced with increasing O_2 concentration and led to fitted rising rates significantly higher (up to a factor of 2) as compared to the OH decay rates (obtained independently from the OH decay curves). On the other hand, within experimental scatter there was no significant deviation from a biexponential time dependence. The question arises if this departure from a fast equilibrium also affects the fitted decay rates.

In Figure 7 an experimental decay curve and numerical simulations (FACSIMILE)[29] are shown which aim to estimate k_{2a} and ${}^1k_{-2a}$. The simulations are based on the results obtained above, i.e., $K_{2a} = 3.25 \times 10^{-19}$ cm^3 and the limiting cases $k_{2b} = 6.0 \times 10^{-16}$ cm^3 s^{-1} or ${}^1k_3 = 1.85 \times 10^3$ s^{-1}. The background of the experimental curve is attributed to a product of the adduct/peroxy radical loss reaction. The rising concentration of this product is also simulated in Figure 7 (upper panel) and its absorption signal is scaled to match the final height of the experimental data. The simulated total absorptions correspond to the sum of adduct and background signals. However, the heights of the adduct signals were not adjusted to the experimental data. They result from the amount of OH produced in the experiment (known from the OH decay curve), the yield of the adduct (dependent on the toluene/H_2O_2 concentration ratio) and the absorption cross section of the adduct. A possible absorption by the peroxy radical is neglected here because it is expected to be minor (see below). In the simulations the rate constants k_{2a} and ${}^1k_{-2a}$ ($= k_{2a}/K_{2a}$) were changed to investigate the influence on the decay curves dependent on the mechanism (loss via Reaction 2b or 3). The results show that a marked deviation from biexponential behavior is evident at $k_{2a} = 1 \times 10^{-15}$ cm^3 s^{-1} if the loss takes place via Reaction 2b. The other curves are essentially biexponential with increased rising rates compared with the OH decay rates. The experimental curve is best represented (signal height and time at maximum) by the simulation with $k_{2a} = 2 \times 10^{-15}$ cm^3 s^{-1} and the loss taking place via Reaction 3. On the other hand, experimental curves at higher O_2 concentration are better reproduced by $k_{2a} \approx 4 \times 10^{-15}$ cm^3 s^{-1}. Thus, $k_{2a} = (3 \pm 2 \times 10^{-15}$ cm^3 s^{-1} is roughly estimated which corresponds to a decomposition rate constant of ${}^1k_{-2a} = (9 \pm 6) \times 10^3$ s^{-1}.

More accurate estimates are not possible due to the uncertainties concerned with the background signal, a possible contribution of a peroxy radical absorption (see below), and the unknown nature of the loss process. However, it should be noted that any absorption by the peroxy radical is expected to decay with the same rate as the adduct, i.e., it would influence the signal height rather than the decay of the curves.

As is evident from the Figure 7 (lower panel), after subtraction of the final background, the decay rates of the curves are only slightly affected by the magnitude of k_{2a}, i.e., the rate constants derived from biexponential fits to the experimental data should, in good approximation, represent the effective rate constants according to eq 8. The deviations can lead to decay rates which are systematically lower by no more than 30%.

Third, Figure 4 shows that there is also a slight tailing of the decay curves which cannot be explained by the factors discussed so far. These deviations could be due to the presence of more than one adduct isomer (and the corresponding peroxy radicals) with slightly different kinetic properties which will be addressed in the Discussion section.

Effective Absorption Cross Sections

The absorption cross sections listed in Table 4 are those of the adduct and the peroxy radicals weighted by their relative concentrations at the different O_2 concentrations. A not ideally fast equilibrium also influences the magnitude of these effective absorption cross sections which would be higher or lower if the loss occurs via the peroxy radical or the adduct (Figure 7). Moreover, it is not clear what fraction of the background must be added to the (extrapolated) absorption signals. If the time behavior of the background is described correctly by the simulations in Figure 7, the background must be added completely. Accordingly, the data listed in Table 4 are containing the background (circles in Figure 6). Also shown in Figure 6 (squares) are the effective absorption cross sections if the background is not added and these data are quite different. Nevertheless, the decrease of the signal with O_2 concentration

can serve as an independent measure for the equilibrium constant. The effective absorption cross sections can be expressed in terms of the absorption cross sections of the adduct (σ_{add}) and the peroxy radical (σ_{per}):

$$\sigma^{eff} = \frac{\sigma_{add} + \sigma_{per} K_{2a}[O_2]}{1 + K_{2a}[O_2]} \quad (10)$$

A fit of eq 10 to the data in Figure 6 yielded $\sigma_{per} = (0.9 \pm 1.3) \times 10^{-18}$ cm^2 and $K_{2a} = (2.6 \pm 0.9) \times 10^{-19}$ cm^3 (2σ error limits) with σ_{add} being held fixed at the value determined in the absence of O_2. If the background signal is not added to the absorption signals the same fits yields $\sigma_{per} = (0.3 \pm 1.5) \times 10^{-18}$ cm^2 and $K_{2a} = (4.1 \pm 1.8) \times 10^{-19}$ cm^3. Thus, although less accurate, the data are consistent with the equilibrium constant obtained from the effective decay rates. If it is assumed that the absorption cross section of the peroxy radical is negligible at 308 nm which is not unreasonable considering typical absorption spectra of peroxy radicals, the expected decrease can be calculated for an equilibrium constant $K_{2a} = 3.25 \times 10^{-19}$ cm^3 (from the effective decay rates). The calculation gave the dashed line in Figure 6 which matches the experimental data reasonably well if the background signal is neglected. However, as mentioned above, the σ^{eff} could be biased toward higher or lower values dependent on the nature of the loss process. Thus, no estimate is made for the absorption cross section of the peroxy radical.

Discussion

Rate Constants of OH + Toluene. The rate constants of the OH + toluene reaction (Table 1) are in good agreement with literature data. Atkinson[2,3] has recommended $k_1(298\ K) = 6.0 \times 10^{-12}$ cm^3 s^{-1} where the review is covering data published before 1994. More recent, partly temperature-dependent[30,31] studies by Semadeni et al.,[30] $k_1(298\ K) = (6.0 \pm 0.3) \times 10^{-12}$ cm^3 s^{-1}, Anderson and Hites,[31] $k_1(298\ K) = (5.8 \pm 1.5) \times 10^{-12}$ cm^3 s^{-1}, and Kramp and Paulsen,[32] $k_1(296\ K) = (5.5 \pm 0.5) \times 10^{-12}$ cm^3 s^{-1}, obtained by relative methods, are also in good agreement with the recommendation by Atkinson[2,3] and the data of this work.

There are two previous determinations of rate constants of OH + toluene-d_8 by Perry et al.[33] and Tully et al.[28] Also in these studies the room-temperature rate constants k_1(toluene) and k_1(toluene-d_8) were similar within their error limits. However, at higher temperatures ($T \geq 400$ K), where the abstraction Reaction 1b dominates, significant differences were observed.[28,33] Tully et al.[28] derived Arrhenius expressions for Reaction 1b for toluene and toluene-d_8. By extrapolation of these expressions, a benzyl radical yield of 2% can be estimated for toluene-d_8 at room temperature, compared with 7% in the case of toluene.[3] Atkinson[2] has given an empirical expression of the kinetic isotope effect of Reaction 1 at elevated temperatures which, extrapolated to room temperature, results in a similar yield of benzyl radicals for toluene-d_8. Thus, the slightly lower k_1 determined for toluene-d_8 (Table 1) can be explained by a lower rate constant of Reaction 1b. However, the difference is not significant within the error limits of the rate constants which are also dependent on a correct vapor pressure determination.

The k_1 measured in N_2 and O_2 are similar for both toluene and toluene-d_8. This means that there are no secondary reactions of the adduct with O_2 leading to a direct regeneration of OH.

Adduct Absorption Cross Section, Adduct Self-Reaction. Markert and Pagsberg[25] determined an absorption cross section of the OH−toluene adduct of $(5.8 \pm 2.0) \times 10^{-18}$ cm^2 at around 300 nm. This cross section was derived from a transient spectrum of products formed by a reaction of similar amounts of OH radicals and H atoms with toluene. The cross-section from Markert and Pagsberg[25] is a factor of 2 smaller than determined in this work, $\sigma_{add}(308\ nm) = (1.1 \pm 0.2) \times 10^{-17}$ cm^2. The reason for the difference is not known.

The absorption cross-section of the OH−benzene adduct determined in ref 16 is about a factor of 2 lower at 308 nm, $(5.8 \pm 1.5) \times 10^{-18}$ cm^2. The relative error of the cross section is higher because the method to obtain OH and adduct absorption signals was improved in this work by pre-triggering the experiment allowing a more accurate determination of experimental background. It should be noted that the correctness of the absorption cross sections is crucial for the determination of the rate constants of the adduct self-reaction and the adduct + HO_2 Reaction 7, i.e., the quantities actually determined in the kinetic experiments are the ratios k_4/σ_{add} and k_7/σ_{add}.

The self-reaction of the OH−toluene adduct has not been studied before. A recently measured rate constant of the self-reaction of the H−benzene adduct (C_6H_7) by Berho et al.[34] is of similar magnitude: $(3.1 \pm 1.0) \times 10^{-11}$ cm^3 s^{-1}, based on $\sigma(C_6H_7) = (2.55 \pm 0.45) \times 10^{-17}$ cm^2 at 302 nm.[34] The rate constant of the self-reaction of the OH−benzene adduct was reevaluated in this work from the data of ref 16 by accounting for the adduct + HO_2 reaction. However, compared with the earlier result[16] the present rate constant is only slightly smaller by about 15% (see Table 3).

While the adduct + HO_2 and adduct + adduct reactions are certainly unimportant for the atmospheric degradation of aromatics, they may be of importance in laboratory studies as has recently been shown by Berndt et al.[35] The rate constant determined in this work for the OH−toluene adduct + HO_2 reaction is very fast: k_7(toluene) $= (1.8 \pm 0.5) \times 10^{-10}$ cm^3 s^{-1}. Since the reaction of HO_2 with OH is comparatively fast (1.1×10^{-10} cm^3 s^{-1})[23] it is assumed that the products of Reaction 7 are toluene, H_2O, and O_2, i.e., toluene is thought to merely enhance the reactivity of the loosely bound OH radical.

Up to now the adduct has been regarded as a single species. However, OH addition to the aromatic ring can proceed at four distinct positions: ortho- (two stereoisomers), meta- (two stereoisomers), para-, and ipso- relative to the CH_3− group. The experiments described here cannot distinguish between these isomers and therefore the determined absorption cross-sections and rate constants are averaged quantities. Theoretical calculations by Bartolotti and Edney[10] and Andino et al.[11] show that the ortho- adduct (Figure 1) is the most stable isomer which is consistent with *o*-cresol dominating in product studies[3] as recently confirmed by Smith et al.[36] and Klotz et al.[8] However, an increased *o*-cresol yield could also be explained by a higher cresol yield of the ortho- adduct + O_2 in Reaction 2b.

Adduct Kinetics in the Presence of O_2. The data presented in Figures 5 and 6 indicate that the reaction of the adduct with O_2 is reversible. Although the peroxy radicals were not detected directly, Figures 5 and 6 show two independent quantities whose dependencies on O_2 concentration are consistent with reversibility. Qualitatively the behavior is similar to that observed with benzene but the loss processes (Reactions 2b and/or 3) are stronger in the case of toluene. The latter result is in accordance with the (effective) rate constants for the adduct + O_2 reactions measured by Knispel et al.,[4] $k_{2b}(300\ K) = (5.4 \pm 0.6) \times 10^{-16}$ cm^3 s^{-1} and Zetzsch et al.,[5] $k_{2b}(295\ K) = (6 \pm 1) \times 10^{-16}$ cm^3 s^{-1}, using resonance fluorescence detection of OH at low O_2 concentrations.

A variety of peroxy radical isomers is possible for each adduct

isomer discussed in the previous section. For example, for the most stable ortho- adduct (Figure 1), three isomeric peroxy radicals are possible (four stereoisomers each). Bartolotti and Edney[10] predicted the peroxy radical with the O_2 in position 3 (ortho- to the OH− and meta- to the CH_3− substituent) as shown in Figure 1 to be the most stable. Andino et al.[11] came to the conclusion that all isomers are equally likely to form and should be considered in the mechanism. With respect to the experiments made here, the existence of peroxy radical isomers means that the measured equilibrium constants and effective loss rate constants correspond to summarized quantities over the *N*-peroxy radical isomers:

$$ {}^1k^{\mathrm{eff}} \approx \frac{[\mathrm{O_2}](k_{2\mathrm{b}} + \sum_{i=1}^{N} K_{2\mathrm{a,i}}\,{}^1k_{3,\mathrm{i}})}{1 + \sum_{i=1}^{N} K_{2\mathrm{a,i}}[\mathrm{O_2}]} \qquad (12) $$

On the other hand, considering the adduct isomers, they are weighted averages if the isomers do not behave too differently. Otherwise this could lead to deviations from simple exponential decays.

For toluene-d_8 the adduct + O_2 reaction has not been studied before. The data show that there is an isotope effect resulting in an effective loss of the adduct about 20% lower compared with toluene. This effect can be attributed to a lowered rate constant of cresol formation by abstraction of a ring D-atom by O_2 (Figure 1) not inconsistent with the typical cresol yield of about 20% obtained with toluene.[3] However, an isotope effect of other possible adduct or peroxy radical reactions (Figure 1) cannot be excluded.

The equilibrium constants K_{2a} are similar for toluene and toluene-d_8. Moreover, the equilibrium constant for benzene, $K_{2a} = (2.7 \pm 0.4) \times 10^{-19}$ cm^3,[16] is similar within the combined error limits. Given the expected strong temperature dependence of the equilibrium constants,[16] this indicates a similar thermochemistry of Reactions 2a/−2a if toluene and benzene are compared.

The experimentally obtained K_{2a} values show that theoretical calculations of the reaction enthalpies are often not precise enough for a reliable prediction of equilibrium constants. Although all calculations are consistent with Reaction 2a being an exothermic process, the predicted reaction enthalpies, $\Delta_r H_{2a}$, vary strongly. In ref 16 it was shown that in the case of benzene the thermochemical data for Reaction 2a ($\Delta_r H_{2a}$, $\Delta_r S_{2a}$) calculated by Lay et al.[17] are in reasonable agreement with the measured equilibrium constant.[16] Atkinson and Lloyd[9] have estimated $\Delta_r H_{2a} = -42$ kJ mol^{-1} for toluene which is comparable with the result of Lay et al.[17] and therefore consistent with the data of this work.

Considering the zero-point vibrational correction by Andino et al.,[11] and using the relation $\Delta_r H_{2a} \approx \Delta_r U_{2a} - RT$, the reaction energies predicted by Bartolotti and Edney[10] lead to a stronger exothermicity inconsistent with the experimentally observed reversibility (also for Reaction 1a).[10] On the other hand, the exothermicity predicted by Andino et al.[11] is smaller and would lead to an equilibrium constant $K_{2a} \approx 1 \times 10^{-24}$ cm^3 (based on an estimated $\Delta_r S_{2a}$ calculated by Lay et al.[17] for the corresponding benzene reaction). Andino et al.[11] argue that the slow rate constant of the adduct + O_2 reaction observed by Knispel et al.[4] ($\approx 6 \times 10^{-16}$ cm^3 s^{-1}) is consistent with their calculated barrier for peroxy radical formation. However, considering the rapid back-reaction (R−2a) forced by the equilibrium constant ($K_{2a} \approx 1 \times 10^{-24}$ cm^3), this would suggest a loss reaction of the order ${}^1k_3 \approx 5 \times 10^8$ s^{-1} (eq 8) making the discussion of a consecutive reaction of the peroxy radical with NO obsolete.

In a recent work by Ghigo and Tonachini[37] a rate constant of 260 s^{-1} is predicted for internal ring-closure of the peroxy radical (III) to give the bridged species (IV) in the case of benzene. This rate constant is in reasonable agreement with the experimentally observed adduct loss[4,5,16] considering the experimentally determined equilibrium constant.[16] However, in the same study a positive free energy change for Reaction 2a is predicted ($\Delta_r G_{2a} = 44$ kJ mol^{-1})[37] from which an equilibrium constant $K_{2a} = 8 \times 10^{-28}$ cm^3 can be calculated, i.e., the equilibrium would be completely on the side of the adduct even at atmospheric levels of O_2. Thus, a rate constant ${}^1k_3 = 260$ s^{-1} would result in a negligible effective second-order rate constant of $k_{2b} \approx 2 \times 10^{-25}$ cm^3 s^{-1} (eq 8).

Nevertheless, the estimated small rate constants of peroxy radical formation for both toluene and benzene[16] $k_{2a} \approx (2-3) \times 10^{-15}$ cm^3 s^{-1}, are in qualitative agreement with a barrier for these processes as predicted by Andino et al.[11] and Ghigo and Tonachini.[18,37]

Recently Molina et al.[38] investigated the intermediates of the OH + toluene reaction in the presence of O_2 by chemical ionization mass spectrometry. A mass peak at $m/e = 141$ was attributed to the peroxy radical (III) while cyclization forming the bridged species (IV) was assumed to be unimportant due to the short residence time.[38] However, at the O_2 concentration used (1×10^{16} cm^{-3}),[38] the results of this work imply that the equilibrium (R2a/−2a) is strongly shifted toward the adduct ([peroxy]/[add] $\approx 3 \times 10^{-3}$). Thus, the probed intermediate is more likely the bridged peroxy radical (IV) or the epoxide−alkoxy radical (VII). On the other hand, formation of a species at $m/e = 173$ corresponding to the peroxy radical (V) was not reported which is inconsistent with the assumption of this work of a fast consecutive formation of this peroxy radical. However, the study by Molina et al.[38] was performed at a low total pressure (1.9 kPa) where the mechanism might be different. Clearly, more work is needed to directly identify the intermediates.

Implications for the Tropospheric Degradation of Aromatics. The results of this work show that under typical tropospheric conditions the peroxy radical (III) is short-lived and will therefore not react with NO, i.e., this reaction pathway can be excluded from the tropospheric degradation mechanism. Since the equilibrium constants measured with benzene and toluene are very similar and rate constants of adduct + O_2 reactions measured for other alkylbenzenes are even higher,[5] this result probably holds for the whole group of alkylbenzenes. However, smog chamber experiments performed at elevated NO levels may have to account for the reaction of the peroxy radical with NO,

$$ \mathrm{adduct{-}O_2} + \mathrm{NO} \rightarrow \mathrm{products} \qquad (R9) $$

and its byproducts (e.g., muconaldehydes).[16]

In ref 16 it has been shown that in the case of benzene a strong influence of temperature on the equilibrium (R2a/−2a) and on secondary product yields can be expected. The same applies for toluene and other alkylbenzenes. For the most important alkylbenzenes temperature-dependent studies of the equilibrium constants are needed to determine the reaction enthalpies of the Reactions 2a. Product yields for example of cresols in the case of toluene as a function of temperature would be an interesting additional information.

In conclusion, important aspects concerning the adduct + O_2 reactions are now believed to be clarified. However, concerning

the consecutive reactions the mechanism of the OH initiated degradation of aromatics remains poorly understood. More work is needed to produce and detect some of the proposed intermediates more directly to clarify the overall mechanism.

Acknowledgment. The experimental work presented in this study was performed at the Fraunhofer-Institut für Toxikologie und Aerosolforschung, Hannover, Germany. Support by this institute is gratefully acknowledged. The work was supported by the Bundesminister für Wissenschaft, Bildung, Forschung und Technologie (BMBF), grant 07TFS30/D3, and by the EC, grant EVK2-CT-1999-00053 (EXACT). The author thanks Prof. C. Zetzsch for useful discussions.

References and Notes

(1) Derwent, R. G.; Jenkin, M. E.; Saunders, S. M. *Atmos. Environ.* **1996**, *30*, 181.
(2) Atkinson, R. *J. Phys. Chem. Ref. Data* **1989**, *Monograph 1*.
(3) Atkinson, R. *J. Phys. Chem. Ref. Data* **1994**, *Monograph 2*.
(4) Knispel, R.; Koch, R.; Siese, M.; Zetzsch, C. *Ber. Bunsen-Ges. Phys. Chem.* **1990**, *94*, 1375.
(5) Zetzsch, C.; Koch, R.; Bohn, B.; Knispel, R.; Siese, M.; Witte, F. *Transport and Transformation of Pollutants in the Troposphere*; Le Bras, George, Ed.; Springer: New York, 1997; Vol. 3, Chapter 3.
(6) Atkinson, R.; Aschmann, S. M. *Int. J. Chem. Kinet.* **1994**, *26*, 929.
(7) Atkinson, R. *Atmos. Environ.* **2000**, *34*, 2063.
(8) Klotz, B.; Sørensen, S.; Barnes, I.; Becker, K. H.; Etzkorn, T.; Volkamer, R.; Platt, U.; Wirtz, K.; Martin-Reviejo, M. *J. Phys. Chem. A* **1998**, *102*, 10289.
(9) Atkinson, R.; Lloyd, A. C. *J. Phys. Chem. Ref. Data* **1984**, *13*, 315.
(10) Bartolotti, L. J.; Edney, E. O. *Chem. Phys. Lett.* **1995**, *245*, 119.
(11) Andino, J. M.; Smith, J. N.; Flagan, R. C.; Goddard, W. A., III; Seinfeld, J. H. *J. Phys. Chem.* **1996**, *100*, 10967.
(12) Klotz, B.; Barnes, I.; Becker, K. H.; Golding, B. T. *J. Chem. Soc., Faraday Trans.* **1997**, *93*, 1507.
(13) Klotz, B.; Barnes, I.; Golding, B. T.; Becker, K. H. *Phys. Chem. Chem. Phys.* **2000**, *2*, 227.
(14) Siese, M.; Koch, R.; Fittschen, C.; Zetzsch, C. *Transport and Transformation of Pollutants in the Troposphere*; Borrell, P. M., Borrell, P., Cvitas, T., Seiler, W., Eds.; SPB Academic Publishing: The Hague, 1994; p 115.
(15) Yu, J.; Jeffries, H. *Atmos. Environ.* **1997**, *31*, 2281.
(16) Bohn, B.; Zetzsch, C. *Phys. Chem. Chem. Phys.* **1999**, *1*, 5097.
(17) Lay, T. H.; Bozzelli, J. W.; Seinfeld, J. H. *J. Phys. Chem.* **1996**, *100*, 6543.
(18) Ghigo, G.; Tonachini, G. *J. Am. Chem. Soc.* **1998**, *120*, 6753.
(19) Pan, X.-M.; von Sonntag, C. *Z. Naturforsch.* **1990**, *45B*, 1337.
(20) Wahner, A.; Zetzsch, C. *J. Phys. Chem.* **1983**, *87*, 4945.
(21) Stephenson, R. M.; Malanowski, S. *Handbook of the Thermodynamics of Organic Compounds*; Elsevier Science Publishing Co.: New York, 1987; and references therein.
(22) Bohn, B.; Siese, M.; Zetzsch, C. *J. Chem. Soc., Faraday Trans.* **1996**, *92*, 1459.
(23) DeMore, W. B.; Sander, S. P.; Golden, D. M.; Hampson, R. F.; Kurylo, M. J.; Howard, C. J.; Ravishankara, A. R.; Kolb, C. E.; Molina, M. J. *Chemical Kinetics and Photochemical Data for Use in Stratospheric Modeling*, Evaluation Number 12; JPL Publication 97-4, Jet Propulsion Laboratory, Pasadena, 1997.
(24) Wahner, A.; Zetzsch, C. *Ber. Bunsen-Ges. Phys. Chem.* **1985**, *89*, 323.
(25) Markert, F.; Pagsberg, P. *Chem. Phys. Lett.* **1993**, *209*, 445.
(26) Bohn, B.; Zetzsch, C. *J. Phys. Chem. A* **1997**, *101*, 1488.
(27) Dorn, H.-P.; Neuroth, R.; Hofzumahaus, A. *J. Geophys. Res.* **1995**, *100*, D4, 7397; Leonard, C. Ph.D. Thesis, University of Hannover, 1990.
(28) Tully, F. P.; Ravishankara, A. R.; Thompson, R. L.; Nicovich, J. M.; Shah, R. C.; Kreutter, N. M.; Wine, P. H. *J. Phys. Chem.* **1981**, *85*, 2262.
(29) FACSIMILE by AEA Technology Harwell, Didcot, U.K., 1993.
(30) Semadeni, A.; Stocker, D. W.; Kerr, J. A. *Int. J. Chem. Kinet.* **1995**, *27*, 287.
(31) Anderson, P. N.; Hites, R. A. *Environ. Sci. Technol.* **1995**, *30*, 301.
(32) Kramp, F.; Paulson, S. E. *J. Phys. Chem. A* **1998**, *102*, 2685.
(33) Perry, R. A.; Atkinson, R.; Pitts, J. N., Jr. *J. Phys. Chem.* **1977**, *81*, 296.
(34) Berho, F.; Rayez, M.-T.; Lesclaux, R. *J. Phys. Chem.* **1999**, *103*, 5501.
(35) Berndt, T.; Böge, O.; Herrmann, H. *Chem. Phys. Lett.* **1999**, *314*, 435.
(36) Smith, D. F.; McIver, C. D.; Kleindienst, T. E. *J. Atmos. Chem.* **1998**, *30*, 209.
(37) Ghigo, G.; Tonachini, G. *J. Am. Chem. Soc.* **1999**, *121*, 8366.
(38) Molina, M. J.; Zhang, R.; Brockhuizen, K.; Lei, W.; Navarro, R.; Molina, L. T. *J. Am. Chem. Soc.* **1999**, *121*, 10225.